REACTION FORCE CANCELLATION WITHOUT A BALANCE MASS

In many precision machines with an internal motion stage, the requirements for throughput and accuracy pose conflicting demands on the system design. In this article, we show that active vibration isolation systems can be used to cancel the reaction forces of a motion stage placed on the payload while simultaneously isolating it from the floor. This cancellation is done in a feedforward manner, and system uncertainties and changes can be tracked by making the feedforward adaptive. The experimental validation shows that it is possible to almost completely remove the part of the payload acceleration that is correlated to the stage motion and the floor acceleration, over a wide frequency band.

SIL SPANJER, ROY KELDER, RUBEN GROOTKARZIJN AND WOUTER HAKVOORT

Introduction

The design of a suspension for a precision machine is governed by balancing the sensitivity to direct and indirect disturbances. Here, direct disturbances are disturbances that act directly on the sensitive part of the machine. These direct disturbances can, for example, originate from cooling. Indirect disturbances are related to the motion of the floor and work on the sensitive part of the machine through the suspension. The motion of the floor is caused by a combination of effects such as seismic activity, traffic and nearby machines.

The sensitivities to direct and indirect disturbances are commonly referred to as compliance and transmissibility, respectively. For passive systems, the balance between the transmissibility and compliance is determined by two trade-offs. The first is the trade-off in the suspension frequency, where lowering the frequency improves the transmissibility, but deteriorates the compliance. The second trade-off is in the relative damping, where a high relative damping reduces the suspension resonance peak in both transmissibility and compliance, but increases the high-frequency transmissibility. These trade-offs can be seen in Figure 1.

The effect of the aforementioned trade-offs can be mitigated when active elements are added to the system. With a combination of feedback and disturbance feedforward, both the compliance and the transmissibility can be improved. Popular choices for feedback are skyhook dampers, due to their effectiveness and robustness.

Many high-performance precision machines include an internal motion stage. These machines often require high accuracy and high throughput. These are conflicting demands, in particular for the suspension stiffness, where a high stiffness is required to counteract the reaction forces for high throughput, while a low stiffness is required to reduce the effect of floor vibrations on the frame for accuracy. A common method to combine both requirements is to add a balance mass to the machine, such that the actuation reaction forces do not enter the machine's sensitive part [1].

Although these balance masses are conceptually simple and have proven to be very effective in practical applications, they come with several downsides. Firstly, properly designed

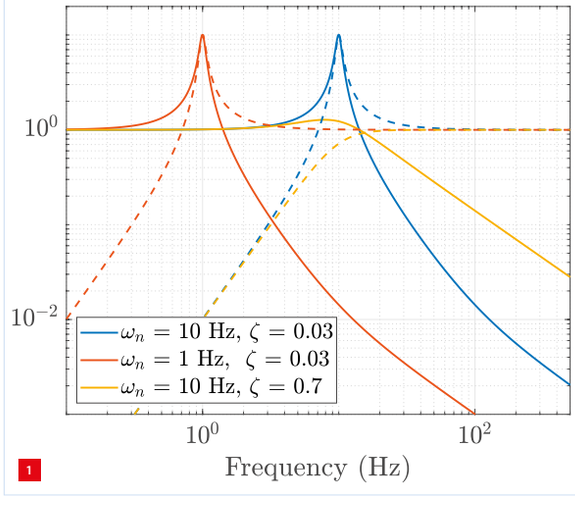

1

Performance trade-offs for a general passive vibration isolation system for the suspension frequency, $\omega_n = \sqrt{(k/m)}$, and relative damping, $\zeta = d/(2m\omega_n)$, with unity mass. Solid lines are transmissibilities, dashed lines are the (double derivatives of the) compliances.

AUTHORS' NOTE

The research described in this article was conducted by Sil Spanjer (Ph.D. candidate), Wouter Hakvoort (associate professor) and the students Roy Kelder and Ruben Grootkarzijn in the chair of Precision Engineering in the Department of Mechanics of Solids, Surfaces & Systems at the University of Twente, Enschede (NL).
The authors would like to thank MI-Partners and PM for their support.

s.t.spanjer@utwente.nl
www.utwente.nl/en/et/ms3

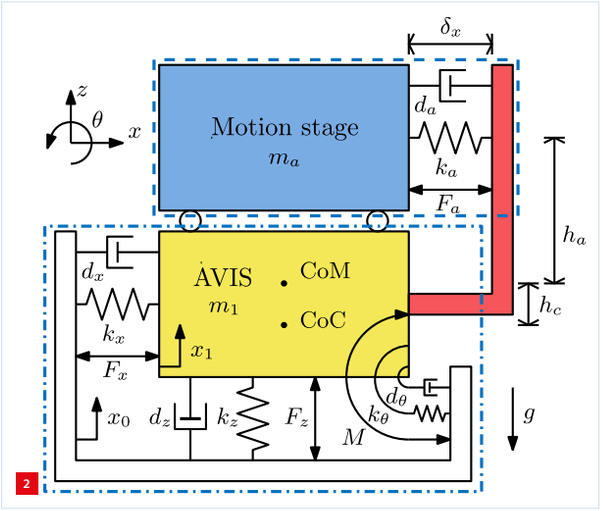

3D representation of the ideal physical model of the AVIS with the internal motion stage.

balance masses are relatively heavy and hence pose strict requirements on the design, and secondly, the implementation of rotational balance masses with sufficient inertia is a considerable design challenge.

As an alternative, active vibration isolation systems (AVIS's) can be used to cancel the reaction forces of the internal motion stage. This has the following advantages:

- No need for additional mass.
- No inherent difference between reaction forces and moments.
- Real-time tracking of system changes.
- Decoupling of the floor motion.

In this article, we first describe the governing dynamics and use these to motivate the controller design. This controller is modified such that it can be implemented adaptively and is thereafter implemented on an experimental system.

System dynamics

Figure 2 shows a three-dimensional ideal physical model (IPM) of the system under consideration. For illustrative purposes, we will focus on this 3D representation for the derivation of the equations of motion and the control laws, while the actual system has six degrees of freedom (6-DoF).

The system consists of a motion stage with mass m_a. This motion stage is placed in a straight guide on the payload mass m_1, which in turn is suspended in springs and dampers from the floor with coordinates x_0. The absolute coordinates of the mass m_1 are x_1. The mass m_1 is actuated with the forces F_x, F_z and the moment M, which are reacted against the floor. The mass m_1, the springs and dampers between m_1 and the floor, and the actuators with the forces F_x, F_z and moment M make up the AVIS. The motion stage is actuated with F_a, which is reacted against m_1. This causes a large disturbance when the stage is in motion. The spring k_a and the damper d_a are placed in the direction of motion of the stage.
The centre of mass (CoM) and the centre of compliance (CoC) of the AVIS are in line with respect to the z-axis on distance h_c. The CoC, also called the elastic centre, is the point where a force in some direction generates a pure translation of that point in the same direction [2]. The CoC does in general not coincide with the CoM.

The linearised equations of motion of this IPM are derived from a nonlinear analysis of the dynamics, and are given by:

$$\boldsymbol{M}\ddot{\boldsymbol{x}}(t) = -\boldsymbol{K}\boldsymbol{x}(t) - \boldsymbol{D}\dot{\boldsymbol{x}}(t) + \boldsymbol{B}\boldsymbol{F}(t) + \boldsymbol{K}_0\boldsymbol{x}_0(t) + \boldsymbol{D}_0\dot{\boldsymbol{x}}_0(t), \tag{1}$$

Here, $\boldsymbol{K}$, $\boldsymbol{D}$ and $\boldsymbol{M}$ are the stiffness, damping and mass matrices, respectively. The matrices K_0 and D_0 are the stiffness and damping matrices related to $\boldsymbol{x}_0$. Equation 1 is parameterised by:

$$\begin{aligned}\boldsymbol{x}(t) &= [\ddot{\boldsymbol{x}}(t) \quad \ddot{x}_a(t)]^{\mathrm{T}} \\ &= [\ddot{x}_1(t) \quad \ddot{z}_1(t) \quad \ddot{\theta}(t) \quad \ddot{x}_a]^{\mathrm{T}} \\ \boldsymbol{F}(t) &= [F_x(t) \quad F_z(t) \quad M(t) \quad F_a(t)]^{\mathrm{T}} \\ \boldsymbol{x}_0(t) &= [x_0(t) \quad z_0(t) \quad \theta_0(t)]^{\mathrm{T}}\end{aligned} \tag{2}$$

$$\boldsymbol{M} = \begin{bmatrix} m_1 & 0 & 0 & 0 \\ 0 & m_1 & 0 & 0 \\ 0 & 0 & I & 0 \\ 0 & 0 & 0 & m_a \end{bmatrix} \tag{3}$$

$$\boldsymbol{K} = \begin{bmatrix} k_x & 0 & h_c k_x + m_a g & -k_a \\ 0 & k_z & 0 & 0 \\ h_c k_x + m_a g & 0 & k_\theta - m_a g h_a & h_a k_a - m_a g \\ -k_a & 0 & h_a k_a - m_a g & k_a \end{bmatrix} \tag{4}$$

$$\boldsymbol{K}_0 = \begin{bmatrix} k_x & 0 & h_c k_x \\ 0 & k_z & 0 \\ h_c k_x & 0 & k_\theta \\ 0 & 0 & 0 \end{bmatrix} \tag{5}$$

$$\boldsymbol{D} = \begin{bmatrix} d_x & 0 & h_c d_x & -d_a \\ 0 & k_z & 0 & 0 \\ h_c d_x & 0 & d_\theta & h_a d_a \\ -d_a & 0 & h_a d_a & d_a \end{bmatrix} \tag{6}$$

$$\boldsymbol{D}_0 = \begin{bmatrix} d_x & 0 & h_c d_x \\ 0 & d_z & 0 \\ h_c d_x & 0 & d_\theta \\ 0 & 0 & 0 \end{bmatrix} \tag{7}$$

$$\boldsymbol{B} = \begin{bmatrix} 1 & 0 & 0 & -1 \\ 0 & 1 & 0 & 0 \\ 0 & 0 & 1 & -h_a \\ 0 & 0 & 0 & 1 \end{bmatrix} \tag{8}$$

The matrix K contains the term $m_a g$ in two elements. This is a mass-stiffness coupling due to gravity, causing a moment if $\delta_x(t) = x_1(t) - x_a(t) \neq 0$. Accelerometers are used to measure the accelerations $\ddot{\boldsymbol{x}}_0(t)$ and $\ddot{\boldsymbol{x}}_1(t)$. A relative displacement sensor is used for δ_x.

Control design

The performance objective of the AVIS with motion stage is twofold. First is to minimise the tracking error and second is the minimisation of the acceleration $\ddot{\boldsymbol{x}}_1$. The tracking error is given by:

$$e(t) = r(t) - \delta_x(t). \tag{9}$$

Here, r is the known reference. To achieve the two performance objectives, consider Equation 1; the last two terms are cancelled with the feedforward controller

$$\boldsymbol{u}_{ff,if}(t) = -\left(\frac{1}{s^2}\boldsymbol{K}_0 + \frac{1}{s}\boldsymbol{D}_0\right)\boldsymbol{a}_0(t), \tag{10}$$

with $\boldsymbol{a}_0(t) = \ddot{\boldsymbol{x}}_1(t)$. This feedforward controller estimates the force exerted on m_1 based on the measurement of the floor acceleration and the knowledge of the suspension dynamics. The subscript 'ff,if' in Equation 10 indicates a feedforward from the floor to the isolated mass m_1.

The feedforward controller from r to the motion stage is the well-known plant inversion:

$$u_{ff,a}(t) = m_a\ddot{r}(t) + d_a\dot{r}(t) + k_a r(t). \tag{11}$$

This feedforward controller is implementable for known second-order continuous reference trajectories. The input force is partitioned as:

$$\boldsymbol{F}(t) = \bar{\boldsymbol{F}}(t) + \begin{bmatrix}\boldsymbol{u}_{ff,if}(t)\\ \boldsymbol{u}_{ff,a}(t)\end{bmatrix}. \tag{12}$$

Substitution in Equation 1 yields:

$$\begin{aligned}\boldsymbol{M}\ddot{\boldsymbol{x}}(t) = &-\boldsymbol{K}\boldsymbol{x}(t) - \boldsymbol{D}\dot{\boldsymbol{x}}(t)\\ &+\begin{bmatrix}1 & 0 & 0 & -1\\ 0 & 1 & 0 & 0\\ 0 & 0 & 1 & -h_a\\ 0 & 0 & 0 & 1\end{bmatrix}\begin{bmatrix}\bar{F}_x(t)\\ \bar{F}_z(t)\\ \bar{M}(t)\\ m_a\ddot{r}(t) + d_a\dot{r}(t) + k_a r(t)\end{bmatrix}.\end{aligned} \tag{13}$$

Let $\bar{\boldsymbol{F}}$ be:

$$\boldsymbol{u}_{ff,ia}(t) = \begin{cases}\bar{F}_x(t) = m_a\ddot{r}(t),\\ \bar{F}_z(t) = 0,\\ \bar{M}(t) = h_a m_a\ddot{r}(t) - m_a g r(t).\end{cases} \tag{14}$$

Substitute this in Equation 13 and neglect the effects of the initial conditions, then

$$\ddot{x}_1(t) = \ddot{z}_1(t) = \ddot{\theta}_1(t) = 0 \tag{15}$$

and

$$\ddot{x}_a(t) = \ddot{r}(t) \tag{16}$$

are the solutions of this system, hence the performance objectives are met. The output $\boldsymbol{u}_{\text{ff,ia}}$ estimates the reaction forces and moments due to the acceleration of m_a and the moment caused by the CoM displacement. These forces and moments are cancelled by the AVIS actuators, and hence are reacted against the floor.

These controllers can be cast into the block scheme in Figure 3, where the realisations of the transfer functions can be inferred from Equation 1. In the top left corner of the block scheme, the classic feedforward feedback motion-control scheme can be seen. The lower right corner is the AVIS. The primary path $\boldsymbol{P}_1(s)$ is the open-loop transmissibility, and the secondary path $\boldsymbol{P}_2(s)$ is the double derivative of the open-loop compliance. The AVIS and motion-control systems are connected via $\boldsymbol{P}_{1,a}(s)$, $\boldsymbol{P}_{4,ai}(s)$ and $\boldsymbol{b}_{ai}(s)$. The subscript 'ai' indicates that the transfer function connects the motion stage (a) with the AVIS (i).

The feedforward controllers are complemented with a feedback controller on the motion stage and a feedback controller on the AVIS. These controllers are used to suppress the unmodelled dynamics and unmeasured disturbances. The motion-stage feedback controller is a PID controller with a cross-over of 120 Hz. The feedback controller of the AVIS is a skyhook damper tuned such that $\zeta \approx 1$ holds for the relative damping of the suspension modes.

In real systems, even with perfect system knowledge, the following approximation holds, due to sampling delays, sensor noise and system limits:

$$\boldsymbol{u}_{ff,if}(t) \approx -\left(\frac{1}{s^2}\boldsymbol{K}_0 + \frac{1}{s}\boldsymbol{D}_0\right)\boldsymbol{a}_0(t), \tag{17}$$

This approximation is efficiently realised by using so-called weak integrators [3]. The feedforward is implemented as an adaptive feedforward to find the best approximation of Equation 17.

Adaptive feedforward

The performance of the feedforward controller depends

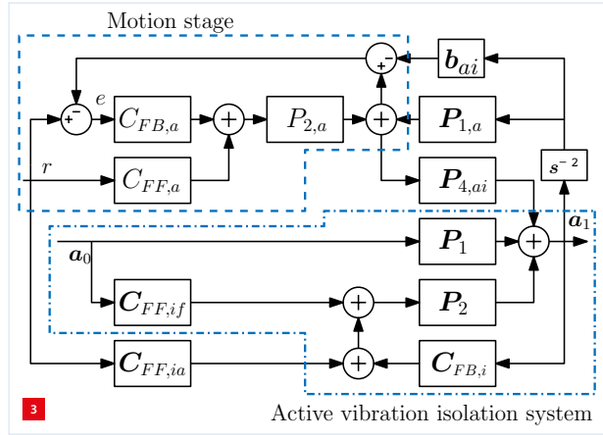

Block-scheme representation of the AVIS (yellow) and the internal motion stage (blue). These are connected with a frame (red).

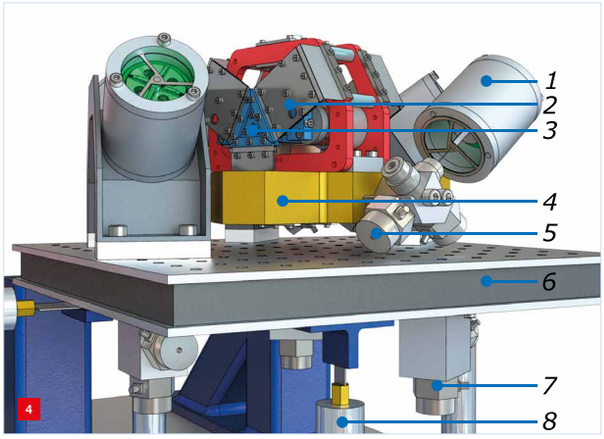

CAD model of the experimental set-up with: 1) VCA, 2) flexure-based straight guide, 3) motion-stage shuttle, 4) payload, 5) payload accelerometers, 6) floor, 7) floor accelerometers, 8) floor shakers. In the CAD model, some components have been left out to better show the motion stage.

on the accuracy of the system parameters. The experimental system uses voltage-controlled voice-coil actuators (VCAs) for the AVIS. The voltage control of the VCA is preferred over current control, for better disturbance behaviour [4]. The use of voltage control makes the motor constant dependent on the temperature of the coil, and hence the (equivalent) parameters of the system drift with temperature.

Furthermore, the parameters that minimise the tracking error and payload acceleration might be different than the actual system parameters due to incompleteness of the model and noisy measurements [5]. The optimal feedforward parameters therefore depend on the reference and the floor spectra. To compensate for these effects, the feedforward is implemented adaptively. As an added benefit in the 6-DoF case, the rotation matrices that relate the principal directions of the system to the sensors and actuators are learned simultaneously.

To implement the adaptive feedforward controller, the Filtered error Adaptive Feedforward (FeAF) method is used in discrete time [6]. The forward shift operator is defined as q, and $t_k = kt_s$, with the index k and the sample time t_s. Details on the derivation of this method have been presented in [3]. FeAF assumes a feedforward controller that is linear in the parameters. This is already the case for the feedforward controllers of Equations 10 and 14 due to the simple dynamics of the system.
The feedforward controllers are combined in:

$$\boldsymbol{u}_{ff,i}(k) = \boldsymbol{u}_{ff,ia}(k) + \boldsymbol{u}_{ff,if}(k) = \boldsymbol{\Psi}(k)\boldsymbol{w}(k). \quad (18)$$

Equation 14 can be rewritten as:

$$\boldsymbol{u}_{ff,ia}(k) = -m_{ia}\ddot{r}(k) - k_{ia}r(k). \quad (19)$$

The total feedforward now becomes:

$$\boldsymbol{u}_{ff,i}(k) = -\underbrace{[\boldsymbol{D}_0 \quad \boldsymbol{K}_0 \quad \boldsymbol{m}_{ia} \quad \boldsymbol{k}_{ia}]}_{\boldsymbol{W}}\underbrace{[\dot{\boldsymbol{x}}_0(k) \quad \boldsymbol{x}_0(k) \quad \ddot{r}(k) \quad r(k)]^{\mathrm{T}}}_{\boldsymbol{\psi}(k)}. \quad (20)$$

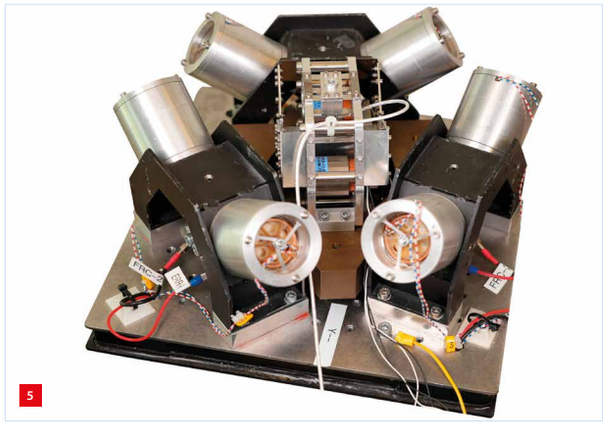

Photo of the experimental set-up.

Note that since $r(k)$ is a design choice, $\ddot{r}(k)$ can be available by design as well. This is not the case for $\dot{\boldsymbol{x}}_0(k)$ and $\ddot{\boldsymbol{x}}_0(k)$ since they are unknown disturbance inputs and, hence, they are observed from the measurement $\ddot{\boldsymbol{x}}_0(k)$. Equation 20 can be rewritten as:

$$\boldsymbol{u}_{ff,i}(k) = -\underbrace{\begin{bmatrix}\boldsymbol{\psi}(k)^{\mathrm{T}} & \dots & \boldsymbol{0}\\ \vdots & \ddots & \vdots \\ \boldsymbol{0} & \dots & \boldsymbol{\psi}(k)^{\mathrm{T}}\end{bmatrix}}_{\boldsymbol{\Psi}(k)}\underbrace{\begin{bmatrix}\boldsymbol{W}_{(1,:)}^{\mathrm{T}}\\ \vdots \\ \boldsymbol{W}_{(3,:)}^{\mathrm{T}}\end{bmatrix}}_{\boldsymbol{w}}, \quad (21)$$

Here, $\boldsymbol{W}_{(1,:)}$ indicates the first row of $\boldsymbol{W}$. Replacing $\boldsymbol{w}$ with $\boldsymbol{w}(k)$ matches the structure to Equation 18. The signals $\boldsymbol{\psi}(k)$ are the basis functions of the feedforward controller.

The weights are updated using a gradient descent method as:

$$\boldsymbol{w}(k+1) = \boldsymbol{w}(k) - \boldsymbol{\Gamma}(k)\boldsymbol{\Psi}^{\mathbf{T}}(k)\varepsilon(k), \quad (22)$$

Here, the filtered error is:

$$\varepsilon(k) = \widehat{\boldsymbol{S}}_2^{-1}(q)a_1, \quad (23)$$

where

$$\widehat{\boldsymbol{S}}_2^{-1}(q) \approx \left[I - P_2(q)C_{FB,i}(q)\right]^{-1}\boldsymbol{P}_2(q), \quad (24)$$

is the model of the process sensitivity, and $\boldsymbol{\Gamma}(k)$ is a suitable gain matrix $\boldsymbol{\Gamma}(k)=\boldsymbol{\Gamma}^{\mathrm{T}}(k) > 0$. This matrix can be determined recursively with a multitude of methods, including Normalized Least Mean Squares (ϵ-LMS), Recursive Least Squares (RLS) and Kalman filtering [7].

Similarly, the feedforward of the motion stage in Equation 11 is written as:

$$u_{ff,a}(k) = -\underbrace{[\ddot{r}(k) \quad \dot{r}(k) \quad r(k)]}_{\boldsymbol{\psi}_a(k)}\underbrace{\begin{bmatrix}m_a\\ d_a\\ k_a\end{bmatrix}}_{\boldsymbol{w}_a}, \quad (25)$$

and the weights are updated using

$$\boldsymbol{w}_a(k+1) = \boldsymbol{w}_a(k) - \boldsymbol{\Gamma}_a(k)\boldsymbol{\psi}_a^{\mathrm{T}}(k)\varepsilon_a(k), \quad (26)$$

with

$$\varepsilon_a(k) = \hat{S}_a^{-1}(q)e(k), \quad (27)$$

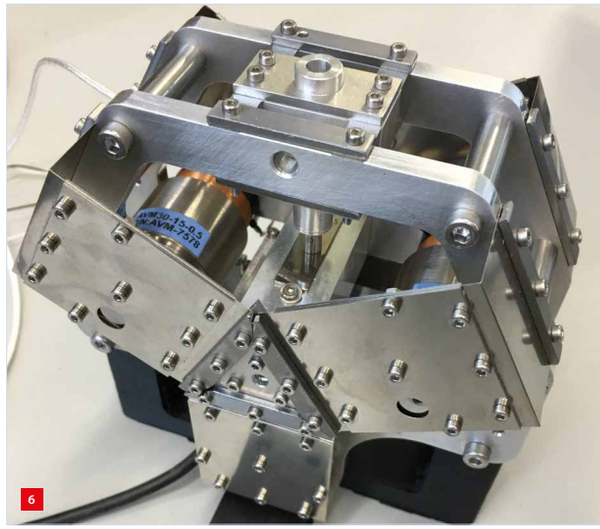

Close-up photo of the motion stage with the flexure-based straight guide.

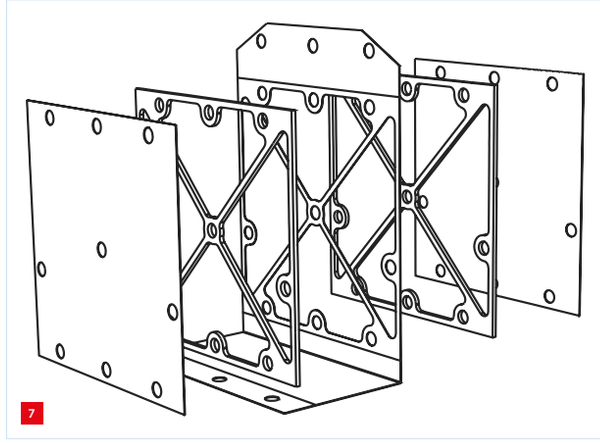

Exploded view of the folded leafspring sandwich structure.

and

$$\hat{\mathcal{S}}_a^{-1}(q) \approx \frac{P_a(q)}{1+C_{FB,a}(q)P_a(q)}. \tag{28}$$

Note that the two update laws of Equations 22 and 26 can be applied simultaneously. This gives the best results due to the feedforward model incompleteness.

System design

For the experimental validation, an existing AVIS was extended with a motion stage. The render of this system is shown in Figure 4 and the realisation can be seen in Figure 5. The AVIS is a 6-DoF, (semi-)hard-mounted system, with suspension frequencies around 24 Hz. The suspended mass of 4 kg is suspended in six wire flexures. These wire flexures connect each to a flexure-based straight guide based on two membrane springs. These membrane springs are connected with a rod to which also the coil of the VCA is connected [2].

On top of the suspended mass is the motion stage, which is a fully flexure-based straight guide. The straight guide consists of two sets of three folded leafsprings. These two sets are connected by the shuttle, which contains the actuators and the relative displacement sensor. The actuators are placed on the (x, y) plane with the centre of mass of the shuttle. The rotation mode around z has been suppressed by choosing a suitable relative gain between the two actuators. The mass of the shuttle is 150 g. A close-up of the motion stage can be seen in Figure 6.

The folded leafsprings have been constructed using a sandwich structure. This sandwich structure increases the internal torsion mode of the reinforcements in the leafspring from 460 Hz in neutral position to 715 Hz. This is the first parasitic mode of the motion stage. Each sandwich structure consists of a folded leafspring with cut-outs. To this, spacers have been added, and the structure is closed with faceplates. An exploded view can be seen in Figure 7. Bolts are used to provide the required clamping force. An additional increase in internal resonance should be achievable using laser welds to connect the different elements.

Experimental validation

The experimental system uses voltage-controlled VCAs in the AVIS. The force output of one actuator is given by:

$$F_a(s) = k_m \frac{\omega_a}{s+\omega_a} V_a(s). \tag{29}$$

Here, ω_a is the frequency of the actuator pole, and V_a the supplied voltage. This introduces additional elements in the feedforward controller since the inverse of the actuator dynamics should be included in the feedforward. For example, Equation 10 becomes:

$$\boldsymbol{u}_{ff,if}(s) = \frac{1}{s^2}(\boldsymbol{A}s + \boldsymbol{I})(\boldsymbol{D}_0 s + \boldsymbol{K}_0)\boldsymbol{a}_0. \tag{30}$$

Here, $\boldsymbol{A}$ contains the poles of the actuator dynamics.

The feedforward controllers have been implemented in six DoFs on the experimental system. For the motion stage, a third-order polynomial reference trajectory is used. This trajectory can be seen in Figure 9 and translates between ±1 mm. One period of the trajectory is 0.2 s, which gives a fundamental frequency of 5 Hz. Only the odd harmonics are present in the input, due to the shape of the reference. This gives a maximal acceleration of about 3.2 m/s^2.

Figure 8 shows the power spectral density (PSD) of the payload acceleration in z and θ_x for two cases. The first case is indicated with 'passive' and has the feedforward of the motion converged, but the controllers of the AVIS turned off. Here the resonance of the AVIS can be seen around 24 Hz. The second case is indicated with 'active' and has all controllers turned on, the feedforward controllers converged and the adaptation stopped after two minutes. This is compared with both the floor spectrum, and the output noise covariance. The output noise covariance is the part of the spectrum $\boldsymbol{S}_{a_1a_1}$ that is uncorrelated with $\boldsymbol{S}_{a_0a_0}$

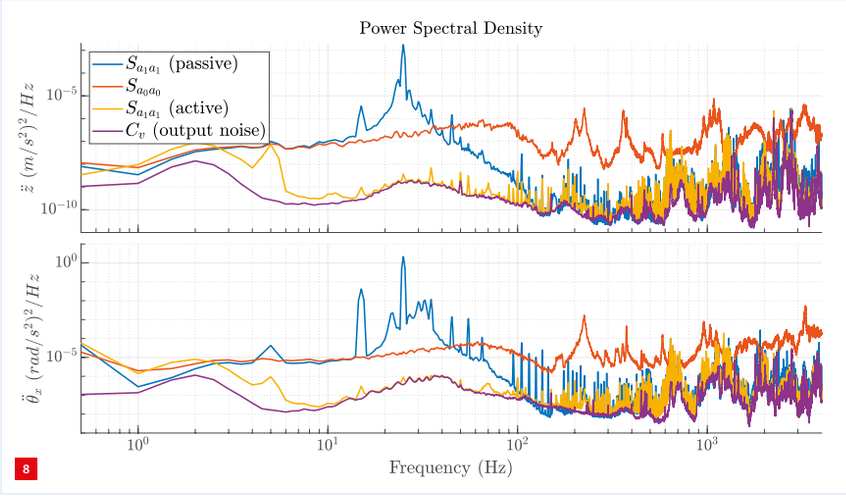

Measured power spectral density (PSD) plots of the platform accelerations, together with the PSD of the floor ($S_{a_0a_0}$) and the output noise. The passive $S_{a_1a_1}$ corresponds with the case where the controllers of the AVIS are turned off, but the motion-stage feedforward and feedback control is turned on. The active $S_{a_1a_1}$ corresponds to all controllers switched on. The output noise is the performance limit of the feedforward controllers.

Table 1
Attenuation of the fundamental and first few harmonics of r on θ_x from the passive to the active case.

Frequency (Hz)	Attenuation (-)
5	45
15	$1.3 \cdot 10^5$
25	$2.4 \cdot 10^6$
35	$1.0 \cdot 10^4$

and S_{rr}, the PSD of a_0, and r, respectively. Hence, it is the performance limit of the feedforward controllers.

The influence of the motion stage is most dominant in θ_x, and can be seen from the peaks at 5 Hz, 15 Hz, etc. In z-direction the peaks are less prominent, which is expected since the z-direction in the IPM is not directly influenced by the motion stage. The obtained acceleration of the payload in the active case is almost equal to the output noise covariance after 10 Hz. This indicates that the feedforward controllers perform optimally. To further improve the performance, the output noise should be lowered. The feedforward controllers improve the PSDs significantly on the interval 5-100 Hz.

The influence of r almost completely disappears on the interval 5-100 Hz with very high suppression factors at the harmonics of the reference. The attenuation of the peak height of the reference fundamental frequency and the first few odd harmonics is listed in Table 1.

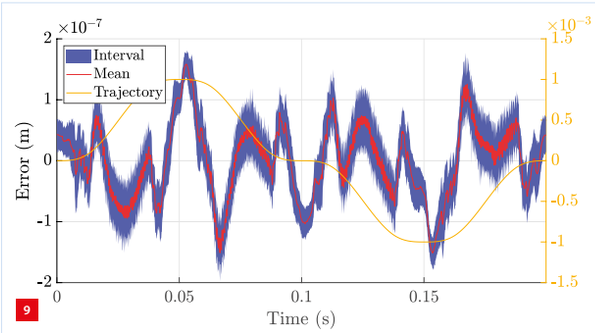

Measured motion-stage error with 900 periods, and the trajectory. All periods are within the indicated interval.

The resulting motion-stage error is displayed in Figure 9 together with the reference trajectory. The error varies on the interval ±180 nm, and still has some structure left. The component of the error in the image of the basis functions, however, has been removed from the data by the feedforward. Hence, an extension of the set of basis functions can improve the error performance. These basis functions should capture the effect of unmodelled dynamics such as hysteresis and nonlinearities in the stiffness. The maximal repeatability of the system is about ±50 nm, hence the error has decreased to less than four times the repeatability. The repeatability is the performance limit of the adaptive feedforward control, independent of the basis function choice.

Conclusion

We propose to use an AVIS as a canceller of the reaction force of the motion stage by transferring the reaction forces to the floor. Implementation of the cancellation using adaptive feedforward control allows to compensate with high bandwidth while changes in the system dynamics can be tracked. The proposed strategy has been implemented on an experimental set-up.

The effectiveness of this method is limited by the resonance modes of the system where the collocation between the motion stage and AVIS actuators or sensors is lost. This limits the usefulness of this method for high frequencies.

REFERENCES

[1] Munnig Schmidt, R., Schitter, G., Rankers, A., and Van Eijk, J., *The Design of High Performance Mechatronics: High-Tech Functionality by Multidisciplinary System Integration,* Ios Press, 2020.

[2] Tjepkema, D., "Active hard mount vibration isolation for precision equipment", Ph.D. thesis, University of Twente, Enschede (NL), 2012.

[3] Beijen, M., Heertjes, M., Van Dijk, J., and Hakvoort, W., "Self-tuning MIMO disturbance feedforward control for active hard-mounted vibration isolators", *Control Engineering Practice*, vol. 72, pp. 90-103, 2018.

[4] Van der Poel, G.W., "An exploration of active hard mount vibration isolation for precision equipment", Ph.D. thesis, University of Twente, Enschede (NL), 2010.

[5] Hakvoort, W.B., and Beijen, M.A., "Filtered error RLS for self-tuning disturbance feedforward control with application to a multi-axis vibration isolator", *Mechatronics*, vol. 89, 102934, 2023.

[6] Spanjer, S., Kelder, R., and Hakvoort, W., "Active vibration isolation with integrated virtual balance mass for a motion stage", In *22nd International euspen Conference & Exhibition, 2022*, pp. 195-198, 2022.

[7] Sayed, A.H., *Fundamentals of adaptive filtering*, John Wiley & Sons, 2003.